

Spatial spectral analysis of human electrocorticograms including the alpha and gamma bands

Walter J. Freeman^{a,*}, Linda J. Rogers^a, Mark D. Holmes^b, Daniel L. Silbergeld^c

^a Department of Molecular and Cell Biology LSA 129, University of California, Berkeley, CA 94720-3200, USA

^b Department of Neurology, University of Washington School of Medicine, Seattle, WA 98104-2499, USA

^c Department of Neurological Surgery, University of Washington School of Medicine, Seattle, WA 98195-6470, USA

Received 20 April 1999; received in revised form 14 September 1999; accepted 9 October 1999

Abstract

Spatial spectral analysis is essential for deriving spatial patterns from simultaneous recordings of electrocorticograms (ECoG), in order to determine the optimal interval between electrodes in arrays, and to design spatial filters, particularly for extraction of information about the dynamics of human gamma activity. ECoG were recorded from up to 64 electrodes 0.5 mm apart in a linear array 3.2 cm long, which was placed on the exposed superior temporal gyrus or motor cortex of volunteers undergoing diagnostic surgery. Visual displays of multiple traces revealed broad spectrum oscillations in episodic bursts having a common aperiodic wave form with recurring patterns of spatial amplitude modulation (AM patterns) on selected portions of the array. The one-dimensional spatial spectrum of the human ECoG was calculated at successive time samples and averaged over periods of up to 20 s. Log power decreased monotonically with increasing log spatial frequency in cycles/mm (c/mm) to the noise level ~ 2 log units below maximal power at minimal frequency (0.039 ± 0.002 c/mm). The inflection point at 0.40 ± 0.05 c/mm specified an optimal value for a low pass spatial filter to remove noise, and an optimal interelectrode spacing of 1.25 mm to avoid undersampling and aliasing. An 8×8 array with that spacing would be 10×10 mm. © 2000 Elsevier Science B.V. All rights reserved.

Keywords: Alpha band; Array recording; ECoG; Electrocorticogram; Gamma band; Spatial frequency sampling; Spatial spectral analysis

1. Introduction

Gamma activity refers to oscillations in the high frequency range of the temporal spectrum of the scalp electroencephalogram (EEG) and electrocorticogram (ECoG) beyond theta (3–7 Hz), alpha (8–12 Hz) and beta (up to 25 Hz), extending to 60 Hz in humans and to 100 Hz or more in small animal species (Bressler and Freeman, 1980). In conformance with an empirical inverse power relation in normal ECoGs (log power decreases by $1/f^b$, $b \sim 2 \pm 1$, with increasing log frequency) (Freeman and van Dijk, 1987; Barlow, 1993; Barrie et al., 1996), the amplitude of gamma activity is usually lower than the amplitudes of the slower components. In humans its modal frequency is in the range of 40 ± 10 Hz. It was first observed in recordings from depth electrodes in the amygdala, where it was associ-

ated with emotional arousal (Lesse, 1957). Numerous investigators have reported finding it in human scalp EEG (reviewed by Sheer, 1989), but verification has been difficult owing to contamination with electromyographic (EMG) potentials having similar temporal spectral properties. Substantial improvements in signal identification techniques applied to EEG records have recently provided strong evidence for the correlation of brief bursts of gamma EEG during cognitive processing in perception and decision making by human volunteers (Müller et al., 1996; Tallon-Baudry et al., 1996, 1998; Miltner et al., 1999; Rodriguez et al., 1999). Its significance is thought to lie in manifesting neural operations by which ‘binding’ of neural activity occurs between networks of neurons separated by relatively great distances in the forebrain, particularly the cerebral cortex of both hemispheres (Milner, 1974; Freeman, 1975; von der Malsburg, 1983; Nunez, 1995; Singer and Gray, 1995; Singer, 1999).

* Corresponding author.

Gamma activity in the ECoG has been studied with rectangular arrays of up to 64 electrodes implanted in cat (Freeman, 1978a; Gaál and Freeman, 1998) and rabbit (Freeman and Schneider, 1982; Freeman and Baird, 1987) in the olfactory system, in the visual cortex of monkey (Freeman and van Dijk, 1987), and the visual, auditory and somatosensory cortices of rabbit (Barrie et al., 1996). The electrodes were spaced typically at intervals of 0.5–0.8 mm. The simultaneous recordings showed that local areas of sensory cortex sustained spatial patterns of amplitude modulation (AM) of a broad spectrum gamma oscillation having a similar aperiodic wave form over the entire array. These patterns of spatial amplitude modulation (AM patterns) formed under classical aversive and appetitive conditioning (Freeman and Schneider, 1982; Freeman and Viana Di Prisco, 1986). The AM patterns took the form of brief gamma bursts lasting ~ 50 – 100 ms episodically between the onset of a discriminative conditioned stimulus (CS) and the conditioned response (CR) at time intervals roughly corresponding to the theta rhythm. Owing to the common wave form, each spatial AM pattern could be expressed as a 1×64 column vector, and as a point in 64-space. Similar patterns gave a cloud of points characterized by a center of gravity ('centroid') and a radius measured by the standard deviation. Classification of the AM patterns was by measurement of the Euclidean distances between points and the respective centroids of distinctive clouds representing discriminative AM patterns formed during presentations of reinforced (CS+) or unreinforced (CS-) stimuli.

An attempt was made to replicate the AM pattern classification results in humans through subdural recordings of gamma activity from the exposed somatosensory cortex under local anesthesia in neurosurgical patients, who were undergoing treatment for intractable epilepsy (Menon et al., 1996). The effort failed, because the 64 electrodes in a standard neurosurgical 8×8 array measuring 8×8 cm were spread over the frontal, temporal and parietal lobes at intervals of 1 cm, and the spatially coherent wave form was found to extend over areas less than 2 cm in diameter. This value was close to the upper limit of the estimated size of coherent domains in animal studies (Freeman et al., 1995).

The design of interelectrode spacing in animal studies was based on spatial spectral analysis of gamma activity at the pial surfaces of the olfactory bulb (Freeman, 1978b; Freeman and Baird, 1987) and of the visual, auditory and somatosensory neocortices (Barrie et al., 1996) in rabbits. Because no prior data were available on the spatial spectrum of the human ECoG, a novel array of 1×64 electrodes was designed and placed for simultaneous recording from a single gyrus, and the data were analyzed to derive a specification for the

optimal spacing of electrodes for spatial AM pattern analysis of human gamma potentials at the subdural cortical surface.

2. Methods

2.1. Spatial sampling

The key requirement for the temporal spectral analysis of digitized time series is that the sampling rate exceed the highest frequency present as a signal in the data, in order to avoid aliasing (misrepresentation at lower frequencies of high frequency components that exceed half the sampling frequency — Gonzalez and Wintz, 1977). In the present series the temporal sampling rate of 420/s (2.38 ms interval, 12 bits/sample) gave a Nyquist (folding) frequency of 210 Hz, which was well above the expected gamma range of 25–100 Hz, after the traces were constrained by the amplifiers between 0.5 and 150 Hz, but excluding frequencies < 200 Hz reported by Buzsáki et al. (1992). Comparably, the spatial sampling rate, which is set by the interelectrode distance in an array, must exceed the highest expected spatial frequency. Studies of the ECoG of rabbit neocortex (Barrie et al., 1996), which has about half the thickness but has cytoarchitectural properties otherwise similar to those in human neocortex (von Economo and Koskinas, 1925; Sholl, 1956), have shown that the highest expected spatial frequency of neocortical gamma activity was between 0.4 and 0.6 cycles/millimeter (c/mm). These estimates were consistent with the depth and 'point spread function' (the width of the bell-shaped distribution at the pial surface of the dendritic dipole field of potential of a single synaptically excited neuron — Freeman, 1975, 1992) of the putative dendritic generators of the olfactory ECoG. Therefore, a 1×64 array was designed with spacing of 0.5 mm between stainless steel electrodes 0.1 mm in diameter, giving a Nyquist frequency of 1.0 c/mm. The array was 32 mm in length, giving a lower spatial spectral limit of 0.031 c/mm, so it could be applied to a single gyrus, typically in humans 1 cm in width and several cm in length, without crossing intervening sulci.

2.2. Spectral analysis

Continuous recordings up to 2 min without behavioral manipulation were visually edited to identify 20 segments 1 s in duration that were free of artifacts. Up to seven electrodes identified as inoperative were replaced by an average of the two traces on adjacent channels. This number was identified by removing channels from intact records and finding no significant effects on spectra with replacement of up to 10% of

channels. For three patients the first 15 electrodes were inoperative, perhaps because of poor electrical contact at the time of surgical placement, so the traces were dropped from the calculations. The remaining values in each time frame were embedded with enough zeroes to give 128 values for the one-dimensional FFT with a Hanning window. They yielded from 7560 to 10 500 spatial spectra for each patient, which were averaged to give mean power spectra depicted in log–log plots. Spatial spectra were also calculated for rms values in selected segments 152 ms in duration (64 time steps), in order to evaluate the effect of averaging over time prior to derivation of the spectra. Principal components analysis (PCA) was also applied to those segments of the data in order to evaluate the degree of spatial coherence

in the data and to extract the spatial modes. Thus, the spatial variables were the 64 electrodes.

Temporal spectra were averaged over three 0.25 s segments stepped at 0.5 s intervals in 1-s epochs from 20 traces for each of the 49 to 64 electrodes. They were embedded in zeroes to give 256 time points, and a Hanning window was applied. Spatial spectra were calculated for each patient after temporal bandpass filtering into ten segments of 5 Hz each, in order to search for spatial spectral peaks associated with temporal concentrations of power, and in order to determine whether the power for high temporal frequencies (beta, gamma) in spatial spectra fell more rapidly with increasing spatial frequency than power for low temporal frequencies (alpha, theta). This finding would be predicted, if the velocity of axonal propagation leading to phase dispersion played a significant role in the formation of spatial AM patterns.

2.3. Subjects

Patient 1 was 43, male, with a meningioma in the left temporal lobe. Recording was in the superior temporal gyrus under propofol anesthesia.

Patient 2 was 18, male, with intractable idiopathic seizures arising in the left posterior temporoparietal cortex. Recording was from the left Rolandic cortex under propofol anesthesia.

Patient 3 was 46, female, with intractable epilepsy following head injury. Recording was from the superior temporal gyrus under propofol anesthesia.

Patient 4 was 43, female, with intractable epilepsy following head injury. Recording was from the superior temporal gyrus under propofol anesthesia.

Patient 5 was 50, male, with left frontotemporal oligodendroglioma and intractable epilepsy. Recording was from the superior temporal gyrus with the patient awake.

3. Results

Examples are shown of ECoG traces from 15 adjacent electrodes placed in a patient under full surgical propofol anesthesia (Fig. 1a) and from an awake patient under local anesthesia (Fig. 1b). They reveal the typical mixture of shared wave-forms of endogenous oscillations at differing amplitudes with electrical noise. The temporal spectra show the typical $1/f^b$ power distribution with $b = 2.32 \pm 0.27$ (S.E.) (Fig. 2). Two of the anesthetized patients (S1 and S3) had a peak at and above the alpha range (here 11–15 Hz). The awake patient (S5) showed strong power in the gamma range (here 25–60 Hz with maximal power between 41 and 45 Hz). Sharp, strong peaks appeared in the high frequency range at 84, 126 and 168 Hz in precise integer

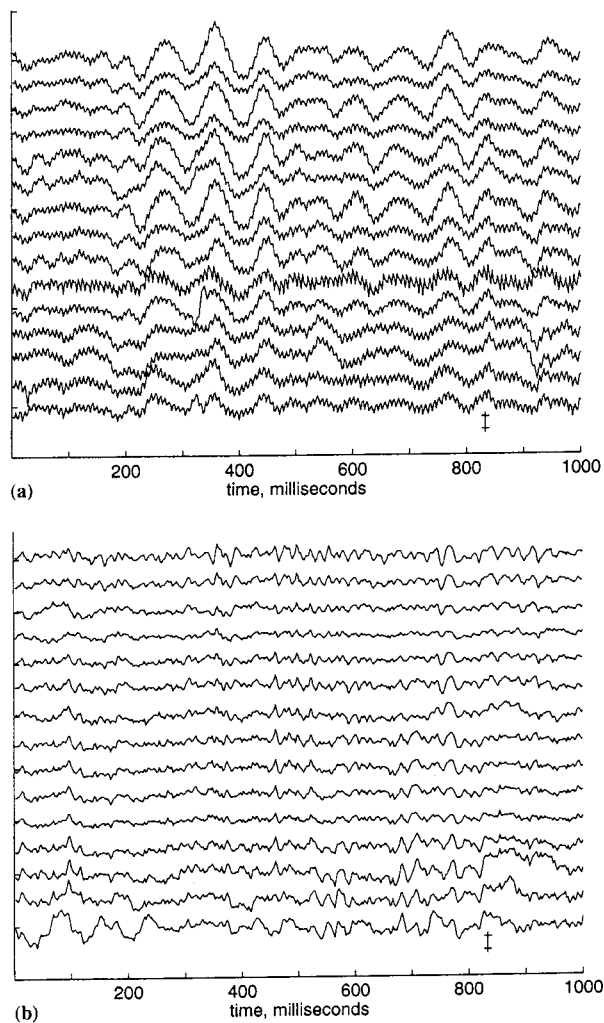


Fig. 1. (a) An example is shown of 15 adjacent traces of ECoG under anesthesia, in which prominent oscillations in the alpha band and ambient electrical noise (Fig. 2c) introduced numerical artifacts into the spatial spectra (Fig. 4c). (b) An example is shown of the ECoG in an awake patient, in which strong gamma oscillations were distributed over the temporal spectrum from 25 to 60 Hz (Fig. 2e). Calibration is 50 μ V. Interval between traces is 100 μ V.

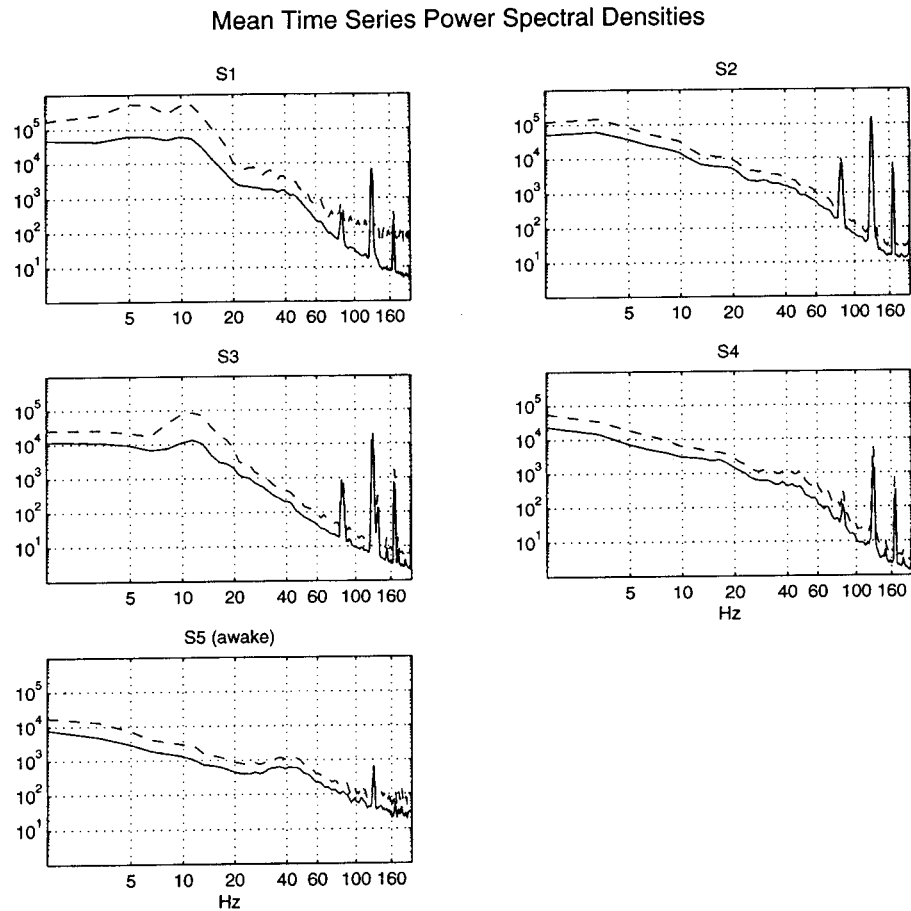


Fig. 2. Temporal spectra (mean and standard deviation, S.D., $N = 7560\text{--}10\,500$) from four anesthetized patients and one awake patient revealed the characteristic $1/f^b$, $b \sim 2$, decrease in log power of ECoG with increasing log temporal frequency, but with strong power in the alpha band of two of the anesthetized patients, in the gamma band of the awake patient, and in spectral spikes from noise in the high frequency band.

ratios, reflecting unavoidable electrical noise with harmonics in the operating theater. The spatial patterns of amplitude, estimated to a first approximation from the root mean square (rms) values of the traces after band pass filtering (5–50 Hz), varied over successive samples but in averages revealed characteristic AM patterns for each patient (Fig. 3, dark traces). Comparison of the gamma AM patterns with the AM patterns of the electrical noise (Fig. 3, light traces) showed that neither of the two components was spatially uniform, but that they had independent distributions. The variance of the noise pattern in samples taken over time was less than that of the gamma patterns.

The spatial spectra were calculated from single time frames and averaged over multiple samples for up to 20 s of recording (Fig. 4a, dark solid traces). The log power after filtering ('low pass', 5–50 Hz) fell with increasing spatial frequency monotonically in a concave-downward curve to ~ 0.4 c/mm and then entered a region of erratic fluctuations about a flat baseline,

which were dissimilar across patients. Spatial spectra of the electrical noise (Fig. 4b, lower right frame showing the noise in S2 after 'high pass' filtering, > 60 Hz) revealed a sequence of troughs and peaks starting above 0.06 c/mm, and extending out to the Nyquist frequency (1.0 c/mm), indicating that these fluctuations in the high spatial frequency range about a horizontal mean value are characteristic of the high intensity narrow band noise (S1 in Fig. 1a and Fig. 2).

Linear regression was used to determine the slope and the intercepts of three segments fitted to the spectral curve between the limits set by the length and spacing of the array. The two inflection points, x and y in c/mm between the descending and baseline segments of the spatial spectra in log–log coordinates, were determined by trial and error (Fig. 4b):

$$\log p = c \quad f < x \text{ c/mm}$$

$$\log p = a + b \log f \quad x \leq f \leq y \text{ c/mm}$$

$$\log p = d \quad f > y \text{ c/mm}$$

where c is maximal mean power, p , at low frequency, f in c/mm, d is mean noise power at high spatial frequency, a is the intercept and b is the slope of the monotonic decrease, and x and y are upper and lower inflection points (Table 1 for five patients).

In order to detect possible relations between spatial and temporal spectra, the spatial spectra were calculated after filtering the multiple time series in ten pass bands, each 5 Hz wide ranging from 1 to 5 Hz up to 45–50 Hz. The spatial spectra shared the same form of monotonic decrease in power with increasing frequency up to the noise level >0.4 c/mm. In the anesthetized patients the slopes of the spectra in the near alpha (11–15 Hz) and gamma (41–45 Hz) ranges were nearly

parallel, with more power at lower temporal frequencies (Fig. 5, dashed curves). In the waking patient (Fig. 5, solid curves) there was more power in the gamma range compared with the anesthetized state in the spatial spectral range from 0.03 to 0.1 c/mm, where it exceeded the power in the intervening beta range. Gamma power fell more steeply to the inflection point at 0.4 c/mm. For the approximation of $1/f^b$, $b = -1.5$ for alpha; $b = -2.5$ for gamma.

Principal components analysis of representative samples of the simultaneously recorded time series gave $50 \pm 4\%$ of the total variance in the 1st factor, $22 \pm 1\%$ in the 2nd factor, $11 \pm 1\%$ in the 3rd factor, and the remaining 17% in the residuals (the degrees of freedom

RMS Amplitude Means, high and low-pass

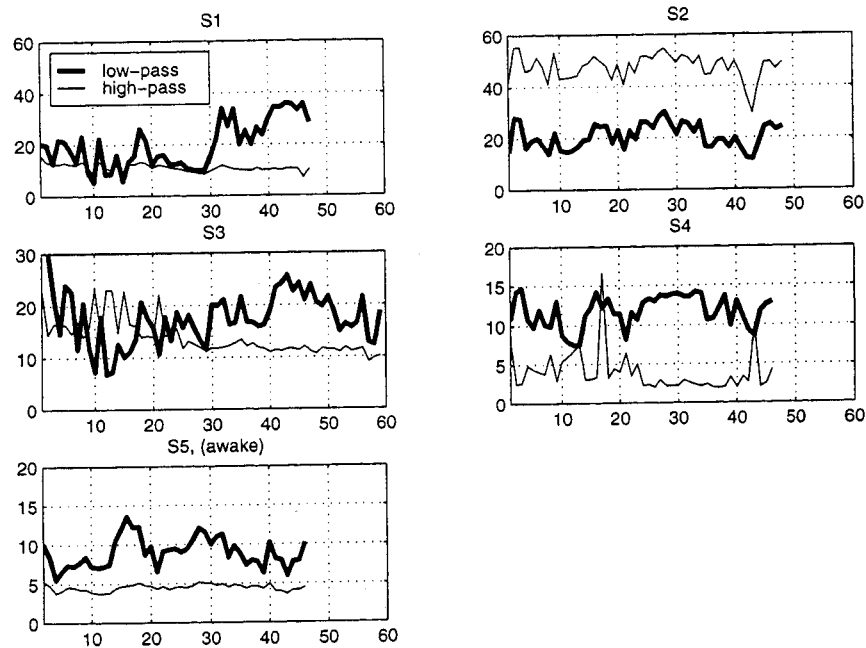


Fig. 3. The spatial patterns across channels (abscissas) of root mean square (rms) amplitude (ordinates) were calculated for the physiological range (5–50 Hz) and for the high frequency range (80–130 Hz), showing that the amplitude of the noise was spatially non-uniform, and that its AM pattern differed from the amplitude pattern in the physiological range, except when the noise was overwhelmingly intense (S2, upper right frame). The mean AM pattern in the 550 Hz range was characteristic for each patient. The scale is in microvolts. Abscissa shows channel number.

Table 1
Evaluation of spatial spectra by linear regression using three line segments^a

Patient	Intercept, a	Slope, b	Max. c	Min. d	Inflection, x	Inflection, y	$c-d$
1	1.36	-1.54	3.50	1.74	0.040	0.56	1.76
2	1.02	-2.27	4.24	1.90	0.038	0.41	2.34
3	1.01	-1.88	3.61	1.82	0.042	0.38	1.79
4	0.41	-2.20	3.70	1.48	0.032	0.33	2.22
5	0.63	-1.95	3.32	1.43	0.042	0.39	1.89
Average	0.89	-1.97	3.67	1.67	0.039	0.41	2.00
\pm S.D.	0.36	0.14	0.15	0.09	0.002	0.03	0.12

^a The slopes and the intercepts at $\log p = 0$ were calculated by curve fitting in log-log coordinates; the abscissa is labeled in linear units. The low standard deviations of the estimates of the inflection points, x and y , were in part due to the discrete grid of the searches for optimal values.

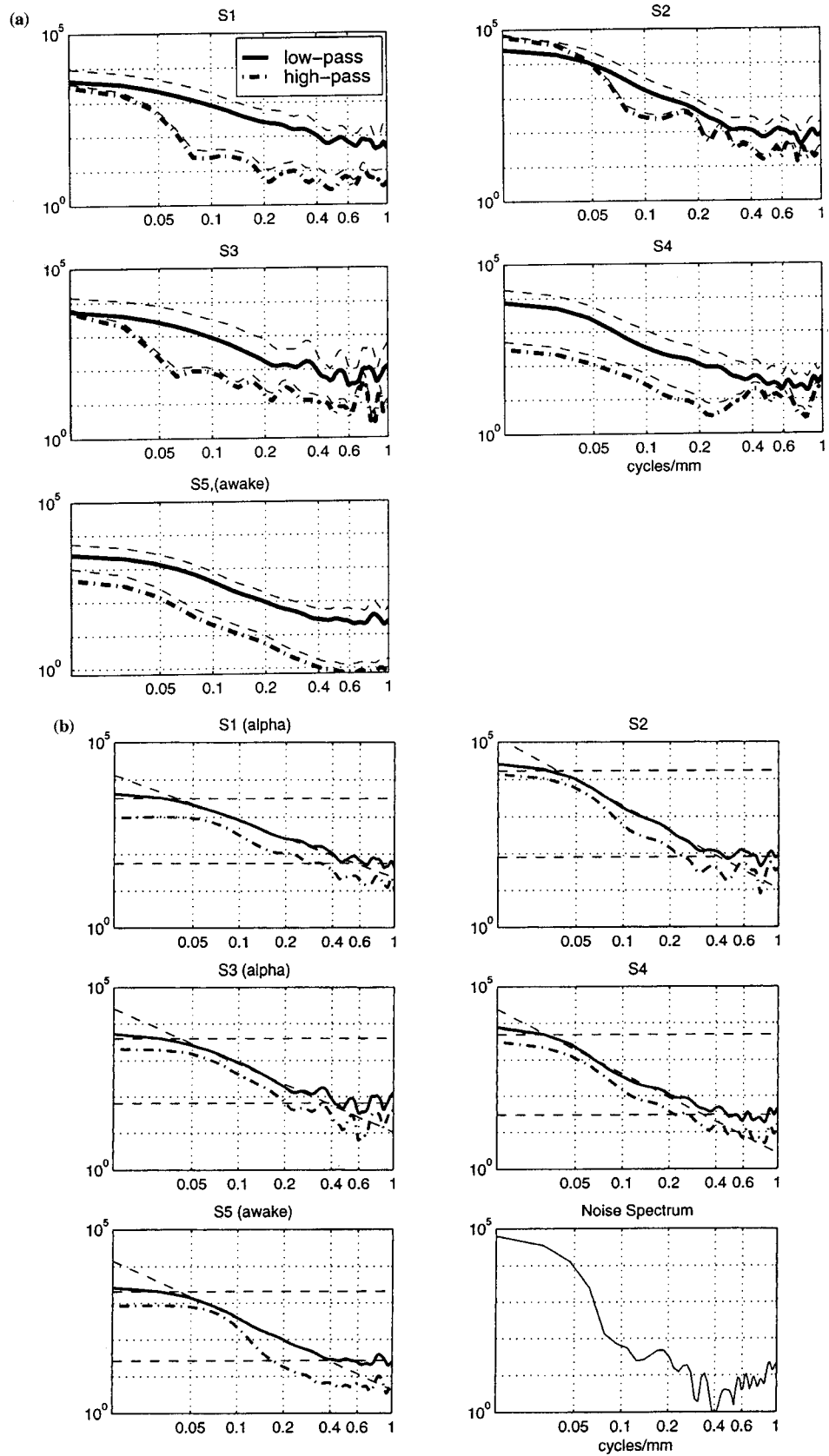


Fig. 4.

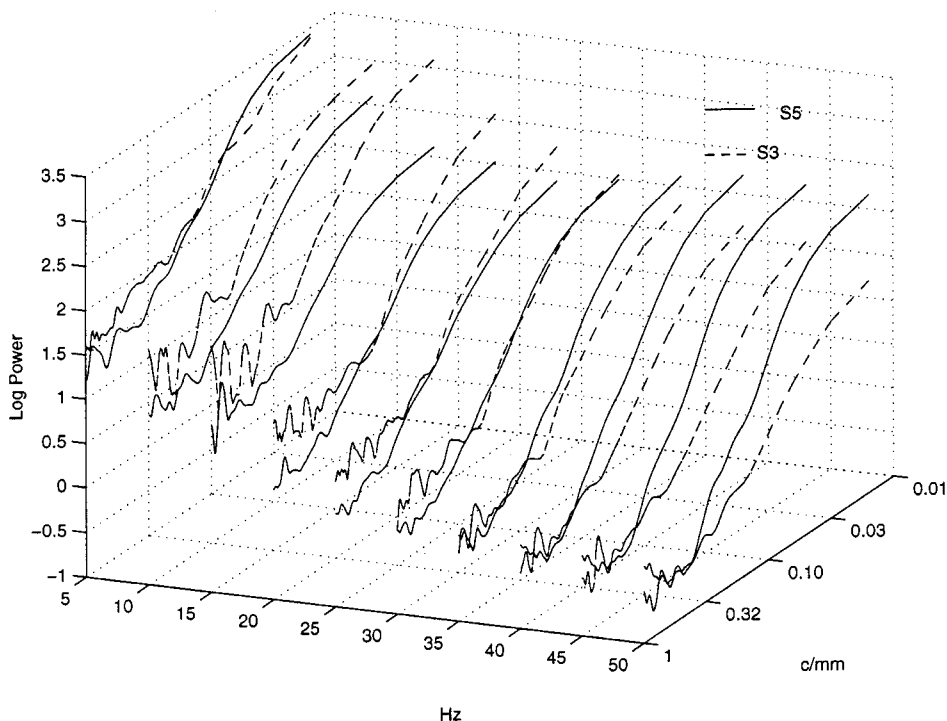


Fig. 5. Dashed curves. Decomposition of the spatial spectrum by analysis of 10 temporal frequency pass bands shows no variation in the distribution of power as a function of spatial frequency with the variation in temporal frequency in anesthetized patients, S1–S4. The peak near 0.3 c/mm disappeared when the spatial digitizing interval was doubled, showing that it was a numerical artifact from digital spectral analysis. Solid curves. Decomposition of the ECoG from an awake patient (S5) revealed strong power in the gamma band at spatial frequencies up to 0.4 c/mm. The frequencies in Hz show the upper limit of the 5 Hz bands.

being 45–64 channels). There were no significant differences between patients in this distribution between factors. The time series of the 1st and 2nd factors for each patient were indeed orthogonal, but their temporal spectra were indistinguishable from each other and from those shown in Fig. 2, apart from the noise peaks. There was no decomposition by temporal frequency. Fig. 6 shows that the spatial pattern of the 1st factor (dark trace) for each patient differed from that of the 2nd factor (light trace). Both traces differed from the rms patterns (Fig. 3), but not significantly, because these were samples of single segments, while the rms were averages over many segments.

The spatial spectra of the 1st component for the

anesthetized patients were lower in power (Fig. 4, dashed traces) but were otherwise not distinguishable from the mean spatial spectra over the time frames. However, in the awake patient (Fig. 4, lower left frame) the power in the range of 0.1–0.4 c/mm was substantially lower for the 1st component than for the spectra without prior temporal smoothing, indicating that use of PCA obscured spatial details by imposing the fixed wave form without phase variation in each factor. The same loss of power in the range of 0.1–0.4 c/mm was found in the spectra computed from rms averages over time segments 152 ms in duration. PCA did appear to bring to the fore the appearance of broad distributions of shared wave forms (Fig. 6, S2 and S5) having widths

Fig. 4. (a) Spatial spectra (mean and S.D.) of the five patients compare the physiological pass band (5–50 Hz, solid curves) with the high frequency noise pass band (~ 60 Hz, dashed curves). (b) Regression lines (Table 1) fitted to the data from the 5 to 50 Hz pass band show the characteristic monotonic fall in log power with log frequency from maximal power to the noise level. The upper inflection point, y , serves to evaluate an optimal low pass filter for removing spatial noise, and to specify an optimal interelectrode distance in arrays for spatial analysis of gamma activity. The lower inflection point, x , provides an estimate of the diameter of the domains of spatial coherence of the broadband oscillations from its reciprocal: < 20 mm. The ratio of the upper to lower plateaus, c/d , gives an estimate of the signal:noise ratio with respect to potential extraction of spatial information from the ECoG. The spatial spectrum of the high frequency noise (f) shows prominent peaks. They are attributable to numerical artifacts in calculating the spectra from digitized values, because their locations are modified by a change in sampling frequency. The dashed curves show the spatial spectra of the 1st factor of principal components analysis (PCA), which is lower in mean power than spectra from instantaneous spatial patterns, but otherwise differs only in the awake patient (S5, lower left frame) at higher spatial frequencies, possibly manifesting phase dispersion detected in AM patterns of neocortical gamma activity in animals (Freeman et al., 1995).

exceeding 10 mm, which were manifested in the spatial spectra by power at frequencies < 0.1 c/mm. The result is consistent with the prior finding in humans by Menon et al. (1996) that cortical areas having shared wave forms are < 2 cm in diameter, and with measurements in rabbit neocortex giving a modal diameter of areas of high correlation between 5 and 10 mm (Freeman et al., 1995).

4. Discussion

Derivation of temporal spectra from time series is a straight-forward mathematical operation, whereas the interpretation of peaks in terms of signal and noise is problematic. In particular the distinction between gamma activity as an expression of cortical operations and other sources of electrical fluctuations can be difficult and in some situations impossible. The ECoG provides one major advantage over the scalp EEG in that muscle potentials (EMG) are not at issue, but other sources remain, particularly in the operating theater. The major criterion used here in temporal spectra was to exclude oscillations persisting in precise integer ratios, because studies in animals have never shown

gamma oscillations to have sub- or super-harmonics (Freeman, 1975, 1992). Similarly, derivation of spatial spectra is an empirical procedure that reveals the pattern of change in power with increasing spatial frequency, the dependence (if any) of the rate of change (the slope, b) on the temporal frequency, the existence of spatial periodic modes (if any), and the inflection points that mark the lower and upper limits of the pass band for optimally resolving spatial signals embedded in high frequency spatial noise. The major criterion used in spatial spectra was to search for a plateau of mean power characteristic of ‘white noise’ at low power above an inflection point, y , and over spatial frequencies approaching the spatial Nyquist frequency. However, spatial spectra do not serve to define neural signals. That can only be done by correlation of spatiotemporal patterns with aspects of behavior (Freeman, 1975; Freeman and Viana Di Prisco, 1986; Freeman and van Dijk, 1987; Barrie et al., 1996). The higher inflection point, y , serves to specify the minimal value for the interval between electrodes in recording arrays, 1.25 mm, and it gives an initial estimate for the design of low pass spatial filters (Rosenfeld and Kak, 1976) to remove spatial noise. The lower inflection

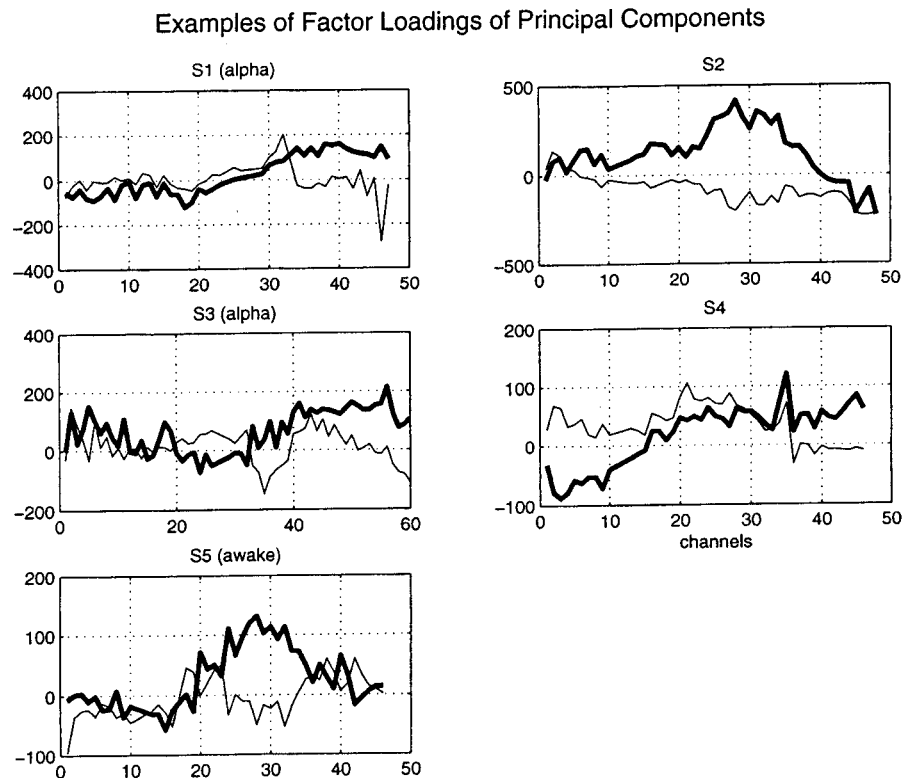


Fig. 6. Principal components analysis (PCA) of representative time segments 152 ms in duration (64 time steps) revealed no decomposition by temporal frequency bands. About half the power was concentrated in the 1st factor with a variable spatial AM pattern (dark traces) both over differing time segments and in comparison to the patterns of the 2nd factor (light traces) and the average AM patterns of instantaneous amplitude (Fig. 3). The further analysis of AM pattern variations will require guidance from behavioral correlation with awake patients.

point, x , gives an indication of the maximal expected size of cooperative domains, for which a suitable array of 64 electrodes would have to be $26 \times 26 \text{ mm}^2$ (the reciprocal of 0.039) to cover the extent of a modal cooperative domain.

The main determinants of the forms of spatial spectra of the ECoG are the depth in the cortex of the layer of neurons generating the synaptic currents, the location of the activating synapses, and the degree of symmetry and mean length constant of the dendrites, whose synaptic currents are the main source of the oscillations in the ECoG. These properties determine the width of the bell-shaped distribution of potential at the pial surface (the point spread function), when a small focus of dendrites is activated, which in turn determines the minimal rate of decrease in spectral power with increasing spatial frequency, that is, the minimal slope, b , of the spectrum (Freeman, 1975, 1978b; Freeman and Baird, 1987). Any source of internal or external driving that coordinates dendritic activity over an area of cortex increases the slope, because the smoothing of local differences in extracellular dendritic potential by excitatory synaptic interaction acts on the ECoG as a low pass spatial filter. If the co-activity is driven by an outside source, such as a thalamic pacemaker, the slope will depend on the lateral dimensions of the thalamocortical afferents (Liley et al., 1999). If the co-activity is self-organized, the slope will increase with the increasing strength of the synaptic connections supporting interactions as they increase the domain size (Freeman, 1992).

The relations between the cytoarchitecture, the point spread function, and the spatial spectrum have been worked out for the ECoG of the olfactory bulb and to a lesser extent the prepyriform cortex (refs. in Freeman, 1975, 1978a), but the neural populations whose dendritic currents give neocortical ECoGs (distinct from ERPs) are not known. The thickness of human neocortex is 2.5–3.0 mm in the superior temporal gyrus and 3.1–3.5 mm in the agranular motor cortex (von Economo and Koskinas, 1925; Sholl, 1956) on the convexities where the present ECoG measurements were made (thickness is half as much in the depths of sulci), compared with 1.5–2.0 mm in neocortex of the rabbit (Thompson et al., 1950), 1.8 mm in the olfactory bulb of the rabbit (Freeman, 1975), 1.3–1.9 mm in the neocortex of the rat (Diamond et al., 1964), and 0.8–0.9 mm in the neocortex of the mouse (Braitenberg and Schüz, 1991). Yet in the species and locations examined so far the spatial spectra show approximately the same slopes and inflection points (Freeman, 1978b; Freeman and Baird, 1987; Barrie et al., 1996), suggesting that the main contributions to the neocortical ECoG in humans come from the pyramidal neurons in layers II and III, which have the requisite packing density, excitatory synaptic interconnections, and dendritic architecture

(Rall, 1995) to give open (dipole) extracellular fields of potential. The layers of these neurons are comparable in depth to those of the generating neurons in the olfactory bulb and prepyriform cortex, for which the zero isopotential plane, as indicated by the ‘turnover’ on depth recording of the ECoG in the bulb and prepyriform cortex, is 0.8–1.0 mm below the pial surface.

Peaks in the spatial spectra might suggest evidence for spatial periodicity in the neural activity patterns manifested in the ECoG. However, in these ECoG data the most likely cause of the peaks at high spatial frequency is numerical artifacts from digital signal processing (Rosenfeld and Kak, 1976; Gonzalez and Wintz, 1977), as shown here by the fact that the peak was abolished simply by using every alternate channel to change the spatial digitizing interval by a factor of two. Such spurious peaks usually occur with digital analysis of intense concentrations of power in narrow frequency bands; when troublesome, their effects are removed by pre-whitening transforms. With one exception the peaks found in the human spectra were 2–4 orders of magnitude less than the low frequency power and were located above the inflection point and near the Nyquist frequency imposed by discrete spatial sampling. One conceivable source of the exceptional peak in two anesthetized patients at 0.3 c/mm for oscillation in the alpha band (Figs. 2 and 4a, S1 and S3) might be aliasing from undersampling of a possible spatial periodicity imposed by the cortical columnar organization. This is unlikely, because the characteristic spatial frequency that could be generated by columns averaging 0.125 mm in diameter is $\sim 2 \text{ c/mm}$, and the attenuation by the point spread function of dendritic generators would be by at least a factor of 10^{-4} at that spatial frequency. Another conceivable source of the peak might be the propagation of alpha waves across the array, so that a temporal frequency would appear as a spatial frequency. The required conduction velocity for a 10 Hz wave to cause a peak at 0.3 c/mm would be 0.033 m/s; there is no apparent physiological explanation for that velocity.

The decomposition of the spatial spectra of the ECoG from anesthetized patients by temporal band-pass filtering revealed no significant dependence on temporal frequency (Fig. 5, dashed curves). The low value of the slope, b , for all temporal pass bands indicated that there was minimal spatial coherence of activity at all temporal frequencies, and that the spatial spectra reflected the properties of the volume conductor, specifically the point spread function of the ECoG generator. Verification of this hypothesis will require depth profile recording as has been done for the olfactory system (Freeman, 1975). The steeper slope for the gamma activity in the awake patient (Fig. 5, solid curves) indicated that a higher degree of spatial coher-

ence accompanied the increased energy in the temporal gamma band, consistent with AM pattern formation. None of the spectra from the anesthetized patients indicated a prominent role for the dispersion relation (Nunez, 1981, 1995), in which AM patterns would have been established by axonal transmission to or in the cortex with fixed velocity, leading to stronger attenuation by phase dispersion at higher temporal frequencies. This may be seen in the difference between the average and the PCA spectra in Fig. 4(b), S5, 0.1–0.4 c/mm. The reason may be that PCA extracts the in-phase component of oscillations into spatial modes, and displays as minor components the effects of phase shift owing to propagation delays. Testing this hypothesis will require spatial filtering of data from 8×8 arrays (Freeman and Baird, 1987). The concave-downward curve of spatial spectra indicated that gamma patterns were due to non uniform activity levels of cortical neurons having a fixed dendritic dipole orientation (Fig. 5 on p. 398 in Freeman and Baird, 1987), in contrast to an alternative model by Katznelson (1982), which assumes uniform activity density of randomly oriented point dipoles and varying local coherence due to local alignment of the dipole moments. This model would give nearly linear spectral curves.

Having data from only one awake patient, we cannot conclude that the difference in spatial spectrum is dependent on the waking state, though the stronger presence of gamma activity in waking as compared with anesthetized states is well documented (Sheer, 1989), but the data show that the method of spectral analysis is worthwhile. The optimal pass bands for observation of the available details in AM patterns in the subdural human ECoG, on the basis of the existing data, are 25–60 Hz in the temporal spectrum and 0.1–0.4 c/mm in the spatial spectrum. The optimal conditions for recording and analysis are a digitizing step of 2 ms and a time window of 128 ms, giving at least three cycles for 25 Hz and at least two measured points in each quarter cycle at 60 Hz, and an electrode interval of 1.25 mm and an 8×8 spatial window of at least 10 mm. These values serve as guidelines to extend the analysis of the human ECoG to two spatial dimensions, and to establish the mesoscopic link between microscopic neural activity in networks and the macroscopic global activity revealed in the scalp EEG (Nunez, 1995; Wright and Liley, 1996; Liley et al., 1999).

Acknowledgements

This research was supported by a Merit Award MH06686, 'Correlation of EEG and Behavior', from the National Institute of Mental Health. We gratefully acknowledge the technical assistance of Julie Rae REEGT, Anthony Bell REEGT, and Leigh Weber

REEGT from the EEG and Clinical Neurophysiology Laboratory, Harborview Medical Center, Seattle WA, and the programming assistance of Brian Burke from the Department of Molecular and Cell Biology, University of California at Berkeley.

References

- Barlow JS. The Electroencephalogram: Its Patterns and Origins. Cambridge MA: MIT, 1993.
- Barrie JM, Freeman WJ, Lenhart M. Modulation by discriminative training of spatial patterns of gamma EEG amplitude and phase in neocortex of rabbits. *J Neurophysiol* 1996;76:520–39.
- Braitenberg V, Schüz A. Anatomy of the Cortex: Statistics and Geometry. Berlin: Springer, 1991.
- Bressler SL, Freeman WJ. Frequency analysis of olfactory system EEG in cat, rabbit and rat. *Electroencephalogr Clin Neurophysiol* 1980;50:19–24.
- Buzsáki G, Horváth Z, Urioste R, Hetke J, Wise K. High-frequency network oscillation in the hippocampus. *Science* 1992;256:1025–7.
- Diamond MC, Krech D, Rosenzweig MR. The effects of an enriched environment on the histology of the rat cerebral cortex. *J Comp Neurol* 1964;123:111–2.
- Freeman WJ. Mass Action in the Nervous System. New York: Academic Press, 1975.
- Freeman WJ. Spatial properties of an EEG event in the olfactory bulb and cortex. *Electroencephalogr Clin Neurophysiol* 1978a;44:586–605.
- Freeman WJ. Spatial frequency analysis of an EEG event in the olfactory bulb. In: Otto DA, editor. *Multidisciplinary Perspectives in Event-Related Brain Potential Research*. U.S. Government Printing Office, EPA-600/9-77-043, 1978b, pp. 531–46.
- Freeman WJ. Tutorial in neurobiology: from single neurons to brain chaos. *Int J Bifurcation Chaos* 1992;2:451–82.
- Freeman WJ, Schneider W. Changes in spatial patterns of rabbit olfactory EEG with conditioning to odors. *Psychophysiology* 1982;19:44–56.
- Freeman WJ, Viana Di Prisco G. EEG spatial pattern differences with discriminated odors manifest chaotic and limit cycle attractors in olfactory bulb of rabbits. In: Palm G, Aertsen A, editors. *Brain Theory*. Berlin: Springer-Verlag, 1986:97–119.
- Freeman WJ, Baird B. Relation of olfactory EEG to behavior: spatial analysis. *Behav Neurosci* 1987;101:393–408.
- Freeman WJ, van Dijk B. Spatial patterns of visual cortical fast EEG during conditioned reflex in a rhesus monkey. *Brain Res* 1987;422:267–76.
- Freeman WJ, Barrie JM, Lenhart M, Tang RX. Spatial phase gradients in neocortical EEGs give modal diameter of 'binding' domains in perception. *Abstr Soc Neurosci* (64813) 1995;21:1649.
- Gaal G, Freeman WJ. Relations among EEGs from the entorhinal cortex, olfactory bulb, somatomotor, auditory and visual cortices in trained cats. In: Ding M, Ditto W, Pecora L, Spano M, Vohra S, editors. *Proceedings of the Fourth Experimental Chaos Conference*. Singapore: World Scientific, 1998.
- Gonzalez RC, Wintz P. *Digital Image Processing*. Reading MA: Addison-Wesley, 1977.
- Katznelson RD. Deterministic and stochastic field theoretic models in the neurophysics of the EEG. Unpublished doctoral dissertation. University of California, San Diego, 1982.
- Lesse H. Amygdaloid electrical activity during a conditioned response. *Proceedings of the 4th International Congress on Electroencephalography and Clinical Neurophysiology*, Brussels, vol. 4, 1957, pp. 99–100.

- Liley DTJ, Alexander DM, Wright JJ, Aldous MD. Alpha rhythm emerges from large-scale networks of realistically coupled multicompartamental model cortical neuron. *Network: Computation in Neural Systems* 1999;10: 79-92.
- Menon V, Freeman WJ, Cutillo BA, Desmond JE, Ward MF, Bressler SL, Laxer KD, Barbaro NM, Gevins AS. Spatio-temporal correlations in human gamma band electroencephalograms. *Electroencephalogr clin Neurophysiol* 1996;98:89-102.
- Milner PM. A model for visual shape recognition. *Psychol Rev* 1974;81:521-535.
- Miltner WHR, Barun C, Arnold M, Witte H, Taub E. Coherence of gamma-band EEG activity as a basis for associative learning. *Nature* 1999;397: 434-436.
- Müller MM, Bosch J, Elbert T, Kreiter A, Valdes Sosa M, Valdes Sosa P, Rockstroh B. Visually induced gamma band responses in human EEG - A link to animal studies. *Exper Brain Res* 1996;112:96-112.
- Nunez PL *Electric Fields of the Brain*. New York: Oxford University Press, 1981.
- Nunez PL (ed.). *Neocortical Dynamics and Human EEG Rhythms*. New York: Oxford University Press, 1995.
- Rall W. *The Theoretical Foundation of Dendritic Function*. Segev I, Rinzel J, Shepherd GM (eds.) Cambridge MA: MIT Press, 1995.
- Rodriguez E, George N, Lachaux J-P, Martinerie J, Renault B, Varela F. Perception's shadow: long-distance synchronization of human brain activity. *Nature* 1999;397: 430-433.
- Rosenfeld A, Kak AC. *Digital Picture Processing*. New York: Academic Press, 1976.
- Sheer DE. Sensory and cognitive 40-Hz event-related potentials: Behavioral correlates, brain function, and clinical application. *Brain Dynamics*. Basar E, Bullock TH (eds.) Berlin: Springer-Verlag, 1989, pp 339-374.
- Sholl DA. *The Organization of the Cerebral Cortex*. London: Methuen, 1956, pp 34-35.
- Singer W. Striving for coherence. *Nature* 1999;39: 391-393.
- Singer W, Gray CM. Visual feature integration and the temporal correlation hypothesis. *Annual Review of Neuroscience* 1995;18:555-586.
- Tallon-Baudry C, Bertrand O, Delpuech C, Pernier J. Stimulus-specificity of phase-locked and non phase-locked 40-Hz visual responses in human. *J Neurosci* 1996;16: 4240-4249
- Tallon-Baudry C, Bertrand O, Peronnet F, Pernier J. Induced gamma-band activity during the delay of a visual short-term memory task in humans. *J Neurosci* 1998;18: 4244-4254.
- Thompson JM, Woolsey CN, Talbot SA. Visual areas I and II of cerebral cortex of rabbit. *J Neurophysiol*. 1950;13:277-288.
- von der Malsburg C. How are nervous structures organized? In E Basar, H Flohr, H Haken & AJ Mandell (eds.), *Synergetics of the Brain*. Berlin: Springer-Verlag, 1983, pp. 238-249.
- von Economo CF, Koskinas GN. *Die Cytoarkitektonik der Hirnrinde des erwachsenen Menschen*. Wien: Springer-Verlag, 1925.
- Wright JJ, Liley DTJ (1996) Dynamics of the brain at global and microscopic scales: Neural networks and the EEG. *Behavioral and Brain Sciences* 19: 285-295.